Influence of P2O5 and Al2O3 content on the structure of erbium-doped borosilicate glasses and on their physical, thermal, optical and luminescence properties

Kevin Bourhis, Jonathan Massera, Laeticia Petit, Heikki Ihalainen, Alexandre Fargues, Thierry Cardinal, Leena Hupa, Mikko Hupa, Marc Dussauze, Vincent Rodriguez, et al.

Influence of P_2O_5 and Al_2O_3 content on the structure of erbium-doped borosilicate glasses and on their physical, thermal, optical and luminescence properties

Kevin Bourhis[a,*], Jonathan Massera[b], Laeticia Petit[c], Heikki Ihalainen[c], Alexandre Fargues[d], Thierry Cardinal[d], Leena Hupa[b], Mikko Hupa[b], Marc Dussauze[e], Vincent Rodriguez[e] , Catherine Boussard-Plédel[f], Bruno Bureau[f], Claire Roiland[f] and Monica Ferraris[a]

[a]*Politecnico di Torino, DISAT, Istituto di Ingegneria e Fisica dei Materiali, Corso Duca degli Abruzzi 24, I-10129, Torino, Italy*

[b]*Process Chemistry Centre, Åbo Akademi University, Biskopsgatan 8, FI-20500, Turku, Finland*

[c]*nLIGHT Corporation, Sorronrinne 9, FI-08500 Lohja, Finland*

[d]*CNRS, Université de Bordeaux, ISM, 351 Cours de la Libération, F-33405 Talence, France*

[e]*CNRS, Université de Bordeaux, ICMCB, 87 Avenue du Dr Schweitzer, F-33608 Pessac, France*

[f]*Equipe Verres et Céramiques, UMR-CNRS 6226, Inst. des Sciences chimiques de Rennes, Université de Rennes 1, 35042 Rennes CEDEX, France*

* Corresponding author. Tel.: +33 540163185. E-mail: k.bourhis@argolight.com (K. Bourhis).

Abstract

The effect of P_2O_5 and/or Al_2O_3 addition in Er-doped borosilicate glasses on the physical, thermal, optical and luminescence properties is investigated. The changes in these glass properties are related to the glass structure modifications induced by the addition of P_2O_5 and/or Al_2O_3, which were probed by FTIR, ^{11}B MAS NMR and X-ray photoelectron spectroscopies. Variations of the polymerization degree of the silicate tetrahedra and modifications in the $^{[3]}B/^{[4]}B$ ratio are explained by a charge compensation mechanism due to the formation of AlO_4, PO_4 groups and the formation of Al–O–P linkages in the glass network. From the absorption and luminescence properties of the

Er^{3+} ions at 980 nm and 1530 nm, declustering is suspected for the highest P_2O_5 concentrations while for the highest Al_2O_3 concentrations no declustering is observed.

Keywords: A. Glasses; C. Infrared spectroscopy; C. Nuclear magnetic resonance (NMR); D. Optical properties; D. Luminescence

1. Introduction

Materials doped with rare-earth (RE) (e.g. Nd^{3+}, Er^{3+}, Yb^{3+}, Tm^{3+}) are of crucial importance in optoelectronics and are widely deployed in fiber amplifiers and solid-state lasers [1,2]. The coincidence between the Er^{3+} emission band around 1530 nm and the principal low-loss window in the absorption spectrum of silicate-based optical fibers has been the main driving force behind much recent work on erbium-doped silica optical fibers and waveguides [2,3]. Intense efforts are on-going worldwide to increase the performances of the Er-doped silica-based fibers used as solid-state lasers and amplifiers. These performances are governed by the relevant electronic and optical characteristics of the active ion, such as absorption and emission cross sections, spectral shapes of the emission and absorption bands, excited state lifetimes, as well as the ion-ion interactions. The host material also has an important impact on all these properties [4,5]. Most of the work reported on Er^{3+}-doped fiber lasers and amplifiers has used high silica-content glasses co-doped with various combinations of Ge, P, and Al atoms [2,3,5]. The main limitations of Er-doped silicate fibers originate from the low solubility of the erbium ions resulting in the formation of Er–Er clusters for the highest erbium concentrations. Er–Er energy transfers most often result in the non-radiative relaxation of the ion pair leading to a quenching of the luminescence at high erbium contents. To prevent such clustering, the fiber core can be additionally doped with alumina or phosphorus pentoxide [6]. It was shown that silica-based glasses should contain at least 8-10 Al or 15 P atoms per rare-earth ion (mainly Yb^{3+} and Nd^{3+}) to prevent RE clustering [7–10]. Moreover, these oxides

have also a significant impact on the silica network [11]. Du *et al.* showed that the introduction of aluminum cations in sodium silicate glasses leads to the formation of negatively-charged $[AlØ_4]^-$ groups, where Ø denotes a bridging-oxygen (bO) atom [12]. A charge compensation mechanism occurs within the glass structure resulting in the transformation of the silicate units with non-bridging oxygen atoms (noted Si-nbO) into units with bridging oxygen atoms (noted Si-bO). The Na^+ ions, previously neutralizing the Si-nbO atoms, are transferred to the $[AlØ_4]^-$ tetrahedra [12,13]. In Na_2O-B_2O_3-SiO_2 (NBS) glasses the charge excess is preferentially compensated by the borate groups and in a lesser extent by the silicate groups, as evidenced by IR [12-17] and NMR spectroscopies [12,18].

Co-doping silica glass simultaneously with Al_2O_3 and P_2O_5 presents an interesting cooperative behavior. Likhachev *et al.* showed that the rare-earth dissolution in the ternary Al_2O_3–P_2O_5–SiO_2 host systems was higher than in the binary P_2O_5–SiO_2 or Al_2O_3–SiO_2 glasses [19]. Although doping with Al_2O_3 or P_2O_5 increases the refractive index (RI) of silica glasses, co-doping the silica glass with Al_2O_3 and P_2O_5 leads to the formation of a glass with a lower RI than that of silica, that the authors related to the formation of $AlPO_4$-like units in the glass network [6,20,21]. The authors stated that such units are created at the expense of $[PØ_4]^-$ and $[AlØ_4]^-$ units, resulting in the formation of Al–O–P linkages with similar bond strength than those in Si–O–Si linkages [20]. This offers the possibility of doping the glass with higher concentrations of P_2O_5 and Al_2O_3 to improve the RE dissolution, thus limiting the RE clustering in the fiber while maintaining a low refractive index. To the best of our knowledge, there have been very few studies on the influence of P_2O_5 and Al_2O_3 on the properties of glasses with a low silica-content.

In this paper, erbium-doped sodium-borosilicate glasses with different Al_2O_3/P_2O_5 ratios have been prepared to better understand the role of P_2O_5 and Al_2O_3 on the Er^{3+} emission properties. The main parameters affecting the luminescence at 1530 nm (absorption properties at 980 nm and

1530 nm, concentration of hydroxyl groups) have been investigated and related to structural modifications of the glass network induced by the introduction of P_2O_5 and/or Al_2O_3.

2. Experimental

2.1 Sample preparation

Glasses having the composition $50SiO_2$-$21.82Na_2O$-$28.06B_2O_3$-$0.12Er_2O_3$ (matrix) and $50SiO_2$-$20.51Na_2O$-$26.36B_2O_3$-$0.12Er_2O_3$-xAl_2O_3-$(3-x)P_2O_5$ (x = 0–3 mol%) were prepared using $NaH_2PO_4.H_2O$ (Merck, 99%), H_3BO_3 (Aldrich, 99.99%), Na_2CO_3 (Sigma-Aldrich, >99.5%), Al_2O_3 (Sigma-Aldrich, >99%), SiO_2 (Sigma-Aldrich, 99%), Er_2O_3 (MV Laboratory, 99.999%) as raw materials in powder form. For the P/Al co-doped glasses, a fraction of the B_2O_3 and Na_2O content is substituted by P_2O_5 and/or Al_2O_3. The compositions of the studied glasses are listed in Table 1. Before melting, the batches were treated at 400 °C for 15 h to completely decompose the raw materials. The batches were then melted in ambient atmosphere in alumina crucibles for 30 min between 1425°C and 1475°C, depending on the glass composition. After quenching on a brass mold, the glasses were annealed for 3 h at 40^{o}C below their respective glass transition temperature (T_g) to remove the internal stress. Finally the samples were cut, ground and polished. The glass compositions were checked by electron-probe micro-analysis and were found to be in accordance with the theoretical ones, within the accuracy of measurement (~ 0.1 wt%). The Er^{3+} concentration is almost the same in all glasses except for the glass matrix for which it is slightly higher.

2.2 Optical measurements

A fully automated Metricon, model 2010 prism-coupled refractometer was used to measure the refractive indices (RI) at 1312 nm, n^{1312}. The accuracy of the measurement is estimated to be ± 0.003. Each measurement was repeated 5 times and at least 3 measurements were performed on different areas of the glass. When the standard deviation (SD) of the measurements was superior to 0.003, the SD was used as uncertainty.

The UV-Vis-NIR absorption spectra were measured on 2 mm-thick samples with a double-beam spectrophotometer (CARY 5000 UV-VIS-NIR) over the 250-2500 nm spectral region. The absorption spectra over the 2500-4000 cm^{-1} range were performed on a FTIR Bruker Alpha-T spectrometer with a spectral resolution of 2 cm^{-1}. The measurements were performed at room temperature and were corrected for the Fresnel losses, which are estimated to be about 7.73-7.67% at 1312 nm (extreme RI values = 1.502 and 1.493). The absorption cross-sections, $\sigma_{abs}(\lambda)$, were calculated from the absorption spectra using Equation (1).

$$\sigma_{abs}(\lambda) = 2.303 \times \log(I_0/I)/(NL) = \alpha(\lambda)/L, \quad (1)$$

where $\log(I_0/I)$ is the absorbance, N the rare earth ion concentration, L the thickness of the sample and $\alpha_{abs}(\lambda)$ the absorption coefficient.

2.3 Thermal and physical measurements

The glass transition (T_g) and glass crystallization (T_x) temperatures were measured by differential thermal analysis (Mettler Toledo TGA/SDTA851) at a heating rate of $15^oC.min^{-1}$. The T_g was taken at the inflection point of the endotherm, as obtained by taking the first derivative of the DSC curve. The T_g was determined with an accuracy of 2^oC. The T_x was taken at the maximum point of the exotherm point. The T_x was determined with an accuracy of 5^oC, and was hardly or not distinguishable in some cases.

The density of the bulk glasses was measured after Archimedes' method in distilled water as an immersion fluid. The accuracy was better than 0.3 %.

2.4 Luminescence measurements

The emission spectra in the 1400–1700 nm range were measured at room temperature using an AOC (Applied Optronics Corp.) laser diode excitation source emitting at 980 nm, an Edinburgh Instruments monochromator (M300) and a liquid nitrogen cooled germanium detector (ADC 403L).

The emission spectra of the samples were collected on powder between quartz plates to avoid reabsorption.

2.5 Infrared spectra measurements

The reflexion infrared spectra were obtained using a Fourier-transform spectrometer (Nicolet 6700 FTIR), by utilizing a 12° off-normal reflection attachment and a high-reflectivity mirror as reference. A proper combination of DTGS detector and beam-splitters (germanium-coated KBr beam splitter or hybrid FIR beam splitter) allowed the measurement of continuous reflectance spectra in the 100–7000 cm^{-1} range. Each spectrum represents the average of 200 scans at 1 cm^{-1} resolution. The spectrometer was purged with dry air to minimize atmospheric CO_2 and water vapor. The reflectance data were analyzed by the Kramers–Krönig transformation to obtain frequency-dependent phase angle between reflected and incident wave. The reflectivity and phase angle spectra were subsequently employed to calculate the optical and dielectric properties of glasses [22]. Infrared data reported in this work are in the form of the absorption coefficient spectra, a, calculated from the relation,

$$\alpha = 4\pi\nu k = 2\pi\nu\varepsilon''/n, \quad (2)$$

where n and k are the frequency-dependent real and imaginary parts of the refractive index, respectively, ε'' is the imaginary part of the dielectric constant and ν is the frequency.

2.6 XPS spectra measurements

The X-ray photoelectron spectra were obtained using a PHI 5000 VersaProbe (PHI Electronics) spectrometer. Monochromatic Al Kα radiation (1486.6 eV) was operated under a residual pressure of 5×10^{-9} mbar. The spectrometer was calibrated using the photoemission lines of Au (Au $^4f_{7/2}$ = 83.9 eV, with reference to the Fermi level). Survey spectra were recorded from 0 to 1400 eV with a pass energy of 187.5 eV using 1 eV steps and four scans. High resolution spectra of

the O1s, C1s and Si2p bands were recorded with a pass energy of 23.50 eV. Scan accumulation enabled to reach a satisfactory signal/noise ratio. Binding energies have been corrected using adventitious hydrocarbon carbon (C1s peak at 284.8 eV) as a reference.

2.7 ^{11}B MAS NMR measurements

Solid State ^{11}B MAS NMR experiments were carried out with a Bruker Avance 600 spectrometer working at 192 MHz for ^{11}B. The spectra were acquired under magic angle spinning (MAS) at a spinning rate of 30 kHz using a 2.5 mm diameter rotor. A 50 kHz radio-frequence field was used for excitation, ensuring an homogeneous and selective excitation of the central transition. A spin echo sequence was used, synchronized on the spinning speed, in order to avoid probe signal and distortion of the baseline. Thus, the delay between two pulses was 33 µs. Besides, it is known that both boron families, the $^{[3]}B$ and $^{[4]}B$ contributions, have different transverse relaxation times (T_2). In order to get some quantitative results, the T_2 were properly measured, $T_2(^{[3]}B)$ = 16 ms, and $T_2(^{[4]}B)$ = 10 ms, and the integrated intensities of each component were corrected following the equation $I_0 = I(t).\exp(t/T_2)$. The chemical shift scale was calibrated with respect to a 1 M B_2O_3 solution. The spectra were reconstructed using the DMFIT software. The model chosen takes into account the spinning sidebands.

2.8 The Dell-Bray-Xiao model

The structure of alkaline borosilicate glasses can be described by the Dell, Bray and Xiao (DBX) model as described in [23]. Using the molar ratios R = SiO_2/B_2O_3 and K = Na_2O/B_2O_3, this model is used to find the fractions of three (N_3) and four (N_4) coordinated boron in each glass after Equations 3–6.

- For $0 \leq R \leq 0.5$ Na_2O converts symmetrical trigonal $^{[3]}B$ into diborate $^{[4]}B$ units. In this range, N_4 is given by

$$N_4 = R \quad (3)$$

- For $0.5 \leq R \leq R_{max}$ (where $R_{max} = 1/2 + K/16$), a borosilicate network starts to form. Additional Na_2O in excess of R = 0.5 is used to destroy diborate groups and creates four loose $^{[4]}B$ units per diborate. Every $^{[4]}B$ unit is then bonded to four Q^4 tetrahedra to form a reedmergnerite ($½(Na_2O.B_2O_3.8SiO_2)$) group. In this range, N_4 is given by

$$N_4 = R \quad (4)$$

- For $R_{max} \leq R \leq R_{d1}$ (where $R_{d1} = 1/2 + K/4$), N_4 is considered as constant and independent of the Na_2O content. The model assumes that all Na_2O in excess of R_{max} are absorbed by reedmergnerite ($½(Na_2O.B_2O_3.8SiO_2)$) groups and form nbO atoms on the silicate tetrahedra. N_4 is given by

$$N_4 = R_{max} \quad (5)$$

Note that for all values of R, N_3 is given by

$$N_3 = 1\text{-}N_4 \quad (6)$$

In P_2O_5-NBS glasses, P_2O_5 is expected to be mainly under the form of $[PØ_3O]^0$ tetrahedra (no pyrophosphate or P–O–P linkage), in analogy with phosphosilicate glasses given the low P_2O_5 fraction (max. 3 mol%) [24]. In Al_2O_3-containing glasses, aluminum oxide has priority to associate itself with an equivalent amount of Na_2O to form $[AlØ_4]^-$ tetrahedra [13–15,25]. The excess Na_2O first associates with borate, as explained above, then with SiO_2 by forming non-bridging oxygen atoms on the Q^4 units. The N_4 values can be estimated by the *R'* parameter, obtained by modifying the R parameter as follows:

$$N_4 = R' = (Na_2O\text{-}Al_2O_3)/B_2O_3 \ (= R'_{max}) \quad (7)$$

The Q^3 and Q^4 silicate units proportion can thus be calculated from Equation 7:

$$Q^3 = (SiO_2\text{-}2Na_2O^{exc})/SiO_2;\ Q^4 = 1\text{-}Q^3 \quad (8)$$

where Na_2O^{exc} is defined as $Na_2O\text{-}(Al_2O_3+2R'_{max}\times B_2O_3)$

3. Results

3.1. Physical properties

The evolutions of the refractive index at 1312 nm and of the glass transition temperature as a function of x are shown in Fig. 1a and 1b, respectively. The addition of P_2O_5 (x = 0) or Al_2O_3 (x = 3) in the glass matrix leads to a decrease of the refractive index. The error bar for x = 0 is quite large since a wide dispersion of the refractive index values was observed for this composition. It can be related to the low solubility of P_2O_5 in silicate-based glasses in agreement with [26]. The refractive index can be considered as almost constant on the composition range, with slightly higher values for x close to 1.5.

The T_g for x = 0 is lowered while it is almost equal to the matrix one for x = 3. A continuous increase of the T_g can be seen when x increases from 0 to 3. The difference $(T_x\text{-}T_g)$ is presented in the inset of Fig. 1b. For the matrix glass, no crystallization peak was detected. The presence of P_2O_5 (x = 0) or Al_2O_3 (x = 3) gives rise to a maximum of $(T_x\text{-}T_g)$ at around 260 °C and 220 °C, respectively. This difference progressively decreases between x = 0 and 3 and reaches a local minimum at around 110 °C for x = 1.67.

3.2. UV-Vis-NIR absorption spectra

A typical absorption spectrum in the UV-Vis-Near IR range of an Er^{3+}-doped glass (matrix) is depicted in Fig. 2a. We found that the UV absorption edge is not clearly affected by x and that the cut-off wavelength remains almost constant at ~ 315 nm. In the 250–1600 nm range, several bands characteristic of the Er^{3+} ion transitions from the ground state to various excited levels are observed. The absorption bands at 980 nm and 1530 nm are represented in Fig. 2b and 2c, respectively. The shape of the band at 980 nm (inset of Fig. 2b) remains almost unchanged while some modifications are observed at 1490 nm and 1530 nm (inset of Fig. 2c) with the addition of P_2O_5 and/or Al_2O_3. The spectral bandwidth is almost constant in both cases (21-23 nm at 980 nm and 24-26 nm at 1530 nm). The evolution of the absorption cross-sections at 980 nm, $\sigma_{abs}(980)$, and of the integrated area

at 1530 nm, $A^{Abs}(1530)$, are plotted respectively in Fig 2d and 2e, respectively. They have very similar evolutions: the introduction of P_2O_5 (x = 0) increases $\sigma(980)$ and $A^{Abs}(1530)$ while these values are similar to the matrix ones when Al_2O_3 (x = 3) is introduced. Both $\sigma_{abs}(980)$ and $A^{Abs}(1530)$ decrease when x increases from 0 to 3. A slight increase of these values is noticed for x ~ 1.5.

The absorption spectra recorded between 3000 and 4000 cm^{-1} are reported in Fig. 3 for some glasses (matrix, x = 0, 1.5 and 3). The spectra show a broad absorption band peaking at around 3500 cm^{-1} usually attributed to OH groups in several oxide glasses [27]. The free OH content can be estimated from the absorption coefficient at 3500 cm^{-1}, α, using Eq. 9

$$[OH] = \alpha \times N_A / \varepsilon, \quad (9)$$

where N_A is the Avogadro constant and ε is the molar absorptivity of the free OH groups in the glass, taken equal to $\varepsilon = 49.1 \times 10^3$ cm^2/mol [28].

The values of α and [OH] for the different glass compositions are listed in Table 1. They are comparable to those reported in several silicate glasses [29,30]. [OH] is close to $5–6 \times 10^{19}$ $ions.cm^{-3}$ for most of the glasses, with slightly higher values for the glasses with x = 0.5 and 1. It has to be noted that [OH] in the P/Al-doped glasses is higher to the one of the matrix glass.

3.3. Luminescence properties

The emission spectra after excitation at 980 nm for some glasses (matrix, x = 0, 1.5 and 3) are depicted in Fig. 4a. They arise from the $^4I_{13/2} \rightarrow {}^4I_{15/2}$ transition typical of the Er^{3+} emission in oxide glasses. As seen for the absorption bands at 1530 nm, the shape of the emission bands depends on the glass composition. The spectral bandwidth remains almost constant upon the composition modification (32-35 nm). The changes in the shape of the emission band (inset of Fig. 4a) were found to be more pronounced in the case of the glasses with $0 \leq x \leq 1.5$. Fig. 4b presents

the variation of the integrated area of the emission band at 1530 nm, $A^{Em}(1530)$, as a function of x. $A^{Em}(1530)$ has a similar evolution as $\sigma(980)$ and $A^{Abs}(1530)$. $A^{Em}(1530)$ strongly decreases when x increases, with a local minimum at x ~ 1.5. The glasses with $x \leq 1$ exhibit a larger emission intensity at 1530 nm than the matrix glass, whereas the glasses with $x > 2$ exhibit a lower emission intensity.

3.4. Structural characterization

The IR spectra in the 250-1600 cm^{-1} range are depicted in Fig. 5a-c. The spectra are composed of broad bands situated in the 400–700, 800–1200 cm^{-1} and 1200–1500 cm^{-1} ranges. The spectra are dominated by an intense band at 1030 cm^{-1} accompanied by shoulders near 900 cm^{-1} and 1150 cm^{-1}. The high-frequency domain exhibits two bands at 1290 cm^{-1} and 1385 cm^{-1} with a shoulder at around 1470 cm^{-1}. In the low-frequency part, a rather intense band at 450 cm^{-1} and a less intense one at around 710 cm^{-1} are visible. As seen in Fig. 5a, the introduction of P_2O_5/Al_2O_3 (x = 0 or 3) in the matrix glass strongly modifies the spectra. Though the position of the most intense band at 1030 cm^{-1} is not significantly affected by the compositional modifications, its width slightly increases on both low- and high-frequency sides. The intensity of the bands in the 1200–1600 cm^{-1} range decreases depending on the glass composition, a minimum amplitude of these bands being observed for the glass with x = 0. In the low frequency part, the intensity of the bands at 450 and 710 cm^{-1} increases, the band at 450 cm^{-1} also becomes sharper for the P_2O_5/Al_2O_3-containing glasses compared to that of the matrix. The intensity of the bands of the glass for x = 1.5 are intermediate between the ones of the -matrix glass and the ones of the P_2O_5/Al_2O_3-containing glasses.

Comparable evolutions are noticed when x increases from 0 to 1.5 and when x decreases from 3 to 1.5. When x increases from 0 to 1.5 or decreases from 3 to 1.5, a widening of the main band at 1030 cm^{-1} is observed when approaching the composition x = 1.5 for which the molar ratio Al/P = 1. The

intensity of the bands in the range 1200–1600 cm^{-1} increases while the amplitude of the bands at 450 cm^{-1} and 710 cm^{-1} slightly decreases when x increases from 0 to 1.5 and when x decreases from 3 to 1.5 (which is less evident for the band at 710 cm^{-1}). It has to be noted that the maximum of the band at 450 cm^{-1} is shifted to higher wavenumbers when x comes close to 1.5.

Fig. 6a presents the Si2p XPS spectra of some glasses (matrix, x = 0, 1.5 and 3). The Si2p spectrum of the glass matrix is composed of a wide band peaking at ~ 102.8 eV. The addition of P_2O_5 (x = 0) and/or Al_2O_3 (x = 3) leads to a shift of the band to higher binding energy (BE). Fig. 6b represents the evolution of the Si2p band maximum as a function of x. When x increases from 0 to 1, the position of the Si2p remains almost constant, then shifts to lower BE when x increases up to 1.67. When x further increases from 1.67 to 3, the Si2p band shifts to higher BE.

The ^{11}B MAS-NMR spectra of some glasses (matrix, x = 0, 1.5 and 3) are presented in Fig. 7a. The two peaks centered at 12 and -1 ppm are attributed to $^{[3]}B$ and $^{[4]}B$, respectively, in agreement with [18,31]. The relative values for both sites as a function of x are presented in Fig. 7b. The $^{[4]}B$ fraction reaches its highest value (60%) for x = 0, decreases to 53% when x increases from 0 to 1.5 (close to the level of the matrix glass) and finally increases when x increases from 1.5 to 3.

The three (N_3) and four (N_4) coordinated boron were estimated using the Dell-Bray-Xiao model as explained in the experimental section. Table 2 lists the N_4, N_3, Q_4 and Q_3 proportion calculated according to the Dell-Bray-Xiao model. Since $R_{max} \leq R' \leq R_{d1}$, the $^{[4]}B$ fraction is expected to be a constant which is in disagreement with the measurement. The DBX model also predicts that the Q^4 fraction increases linearly when x increases (see Fig. 8).

4. Discussion

4.1. Evolution of the refractive index and of the glass transition temperature

The refractive index depends on the overall polarizability of the glass matrix. P and Al are less polarizable than Na. Therefore the observed decrease of refractive index might be due to the partial replacement of Na_2O by P_2O_5 or Al_2O_3.

The lower T_g for x = 0 than for x = 3 can be explained by the number of bonding oxygen atoms born by the P or Al atoms. When P_2O_5 is introduced in the glass (x = 0) $[P\emptyset_3O]^0$ units are formed, whereas when Al_2O_3 is introduced in the glass (x = 3) $[Al\emptyset_4]^-$ groups are formed. The 3-bonded $[P\emptyset_3O]^0$ units, with one terminal atom, weaken the network compared to the 4-bonded $[Al\emptyset_4]^-$ units, giving rise to a glass with a higher T_g for x = 3

4.2. Evolution of the glass structure as a function of x

The structure of sodium-borosilicate glasses is generally described as mixed silicate and borate networks [18,32–37]. Borate groups appear to exist largely as polymerized trigonal $^{[3]}B$ and tetragonal ($^{[4]}B$) units and silicate units as tetrahedral SiO_4 units (Q^n), where n is the number of bO atoms [12,17,38–42].

In the IR spectrum of the glass matrix (Fig. 5a), the main band at 1030 cm^{-1} is associated to the Si–O asymmetric stretching vibrations of the Q^n groups, superposed with the asymmetric stretching vibrational modes of Si–O–B and B–O–B bridges at around 1080 cm^{-1} and 1250 cm^{-1} [33,35,40–44]. The shoulder in the 900-1000 cm^{-1} range is related to the symmetric stretching of the Si–O–$^{[4]}B$ and $^{[3]}B$ –O–$^{[4]}B$ vibrations modes superposed to the asymmetric stretching of the $[B\emptyset_4]^-$ tetrahedra [16,40–42,44,45]. The two bands at 1270 cm^{-1}, 1385 cm^{-1} and the shoulder at 1470 cm^{-1} are related to the asymmetric stretching vibrations of various $^{[3]}B$ units in different ring and non-ring configurations [13,34,35,42,45]. The band of low intensity at 710 cm^{-1} is related to the bending modes of the Si–O–Si, Si–O–B and B–O–B linkages and can be superposed to the bending vibrations of $^{[3]}B$ units [13,22,34]. The low-frequency envelope in the 400–550 cm^{-1} arises from the

rocking motion of Si–O–Si linkages as well as deformation modes of various borate species [13,22,35,45,46]. The introduction of P_2O_5 (x = 0) or Al_2O_3 (x = 3) in the glass matrix leads to the formation of $[P\emptyset_3O]^0$ and $[Al\emptyset_4]^-$ units, which present typical absorption bands at ~ 970 cm^{-1} [47] and at ~ 900 cm^{-1} [13], respectively, corresponding to the vibrations of the Si–O–(Al,P) linkages. Given the low P_2O_5 fraction (max. 3 mol%), phosphate atoms are expected to be mainly under the form of $[P\emptyset_3O]^0$ tetrahedra (no pyrophosphate or P–O–P linkage), in analogy with phosphosilicate glasses [24]. The introduction of such units have an impact on the structure of the glass: the addition of P_2O_5 or Al_2O_3 at the expense of Na_2O and B_2O_3 leads to a glass network with a larger amount of bO atoms on the silicate groups than in the glass matrix as suspected from the shift of the Si2p BE band to higher energy which is in agreement with the Dell-Bray-Xiao model (See Fig. 8). One can notice that the addition of P_2O_5 or Al_2O_3 also leads to an increase in $^{[4]}B$ (Fig. 7b). As explained in [12–16,18], these changes in the glass structure are suspected to be related to a charge compensation mechanism taking place to neutralize the negative charges of the $[Al\emptyset_4]^-$ units. These changes in the glass network result in a larger amount of OH groups as shown in Fig. 3

When x increases from 0 to 1.5 or decreases from 3 to 1.5, the Si2p band shifts to lower BE indicating the formation of a less polymerized silicate network. This hypothesis is also comforted by the shift of the IR band at 470 cm^{-1} when x increases from 0 to 1.5 or decreases from 3 to 1.5. It also leads to a decrease in $^{[4]}B$ (Fig. 7b).

These changes in the glass structure are not in agreement with the evolutions predicted by the Dell-Bray-Xiao model. The Q^4 fraction is expected to increase linearly as illustrated in Fig. 8 and N_4 are supposed to be x independent in disagreement with our measurements. The discrepancy between the prediction of the DBS model and our results, can be explained by the fact that P_2O_5 not only leads to tri-bonded $[P\emptyset_3O]^0$ units but also to charged $[P\emptyset_2O_2]^-$ units. Such units thus have the same behavior as $[Al\emptyset_4]^-$ units and also need to be charge-compensated when present in the glass. Assuming that the P_2O_5 is only present under the form of $[P\emptyset_2O_2]^-$ units, the amount of negatively-

charged units brought by P_2O_5 and Al_2O_3 is similar independently for x = 0 or 3. However the presence probability of such units in the glass is low. Several authors reported the formation of $AlPO_4$ structural units when P_2O_5 and Al_2O_3 are introduced in pure silica glass network. The pure $AlPO_4$ crystal consists of a [PO_4^{3-}] network isolated by Al^{3+} cations [48,49]. The presence of such units in the glass network was suspected due to an improvement of the optical properties such as fluorescence enhancement or the decrease of the refractive index of the glass [6,8,11]. Here, the P_2O_5- and Al_2O_3-containing glass networks are suspected to contain simple isolated Al–O–P linkages rather than crystalline $AlPO_4$ units. Such units exhibit infrared absorption bands located at 730 cm^{-1} and at 1130 cm^{-1} according to [48,49], which eventually contribute to the appearance and increase in intensity of shoulders on both sides of the main absorption band (Fig. 5).Since Al–O–P linkages in $AlPO_4$ units have similar bond strengths than the SiO_4 units [20] their presence in the glass network is expect to lead to a small increase in T_g (Fig. 1b). It is also supported by the strong decrease in the (T_x-T_g) difference at around x ~ 1.5 (Inset of Fig. 1b), indicating the high tendency of the glass x=1.5 to crystallization that may be due to a higher number of Al–O–P linkages.

The DBX model was modified to take into account the formation of such linkages by simulating the formation of $AlPO_4$ units. In this hypothesis the simultaneous presence of Al_2O_3 and P_2O_5 leads to the formation of two $AlPO_4$ units, so that there is one more Na_2O free to interact with the borosilicate network. Therefore, R', defined in Equation 8, can be modified as follows:

$$R^* = (Na_2O\text{-}Al_2O_3\text{-}P_2O_5+2\times AlPO_4)/B_2O_3 \quad (10)$$

The Q^3 and Q^4 silicate units proportion can thus be calculated from Equation 11:

$$Q^3 = (SiO_2\text{-}2Na_2O^{exc})/SiO_2 = 2\times(R^*\text{-}R_{max})/K;\ Q^4 = 1\text{-}Q^3 \quad (11)$$

It can be seen in Fig. 8 that the modified DBX model simulating the formation of $AlPO_4$ groups shows modification of the silicate network evidenced by XPS spectroscopy, but is able neither to give a quantitative analysis of the Q^n group distribution not a good description of the borate network changes induced by the increase of x. Because phase separation can exist between the borate and

the silicate network at the microscopic scale, it is possible to think that P_2O_5 and/or Al_2O_3 enter preferentially in the silicate or in the borate network, giving rise to discrepancies between the measured and predicted structure.

Na^+, $[P\O_4]^0$ and $[Al\O_4]^-$ not only act on the silicate network, as predicted by Dell and co-workers, but also on the borate network.

The two $^{[3]}B$ and $^{[4]}B$ coordinations can be combined to form different groups like boroxol rings, orthoborate, pentaborate, tetraborate, metaborate and diborate groups, etc. The $^{[4]}B$ units give rise to tetrahedral network features in the glass structure, where BO_4 units are always negatively charged ($[B\O_4]^-$), whereas $^{[3]}B$ units may be present as neutral $[B\O_3]^0$, charged units $[B\O_2O]^-$, $[B\OO_2]^{2-}$ or even $[BO_3]^{2-}$) [50].

P_2O_5 has been assumed to form only neutral $[P\O_4]^0$ units, so that the number of nbO in the glass should be unchanged for the matrix glass and for x = 0. Since an increase of the Si BE and of the $^{[4]}B$ content is observed, it is possible to conclude that some part of the nbO atoms born by the silicate network is transferred to the borate network. A fraction of $^{[3]}B$ units may thus be present as charged $[B\O_2O]^-$ (metaborate) units. Given the large variation in the $^{[4]}B$ fraction, it seems reasonable to suggest that phosphate groups enters preferentially the borate network. One cannot exclude the formation of $[P\O_3O]^-$ units requiring Na^+ ions for charge compensation, which would slightly increase the amount of nbO atoms.

On the aluminate-rich side for x = 3, the $[Al\O_4]^-$ groups formed when Al_2O_3 is introduced are charge-compensated by some Na^+ ions, leading to a higher amount of bO atoms in the glass network. The slight increase of $^{[4]}B$ fraction compared to the large XPS shift to high BE may indicate that the created bO atoms are born in a large extent by the silicate network, and in a lesser extent by the $^{[3]}B$ units under the form of neutral $[B\O_3]^0$ units.

When P_2O_5 and Al_2O_3 are mixed the silicate network is depolymerized as indicated by the downshift of the Si BE, while the equilibrium $^{[4]}B \leftrightarrow {}^{[3]}B$ is shifted to the right. Since the formation of $AlPO_4$ units is not a satisfying explanation, one may suggest that when only one dopant (P_2O_5 or

Al_2O_3) is introduced, it is preferentially present in the phase with which it has an affinity. In the case of the mixed P_2O_5/Al_2O_3 glasses the assumptions made above do not explain the observed tendencies of the IR, XPS and NMR measurements. When approaching the composition x = 1.5 the number of nbOs should be reduced compared to the aluminate-rich phase, and should be increased compared to the phosphate-rich phase. That is why it is possible that phosphate and aluminate group interact at the frontier of the silicate and borate phase domains, thus locally affecting both networks. Other hypothesis may also explain some features, such as the formation of alumina-rich domains, as suggested by Monteil et al. by molecular dynamics [51]. Correlative multi-nuclei NMR studies may help solving these issues.

4.3. Influence of the structure on the emission properties

As seen in Fig. 2b-e and 4, the addition of Al_2O_3 and/or P_2O_5 has a strong impact on the absorption and emission properties of Er^{3+} ions. The changes in the shapes and intensities of these bands tend to indicate that the Al and P atoms most probably participate to the second coordination shell around the Er^{3+} ions, while being progressively introduced in the borosilicate glass matrix. Similar changes in the surrounding environment of Er^{3+} after the introduction of P_2O_5 in sodium aluminosilicate glasses have been reported elsewhere [52]. The decrease of the absorption cross-sections at 980 nm and of the absorption intensity at 1530 nm (Fig. 2d and 2e) traduces a lowering of the 4f-4f transitions probabilities when x increases from 0 to 3. Therefore the Er^{3+} site is expected to be less non-centrosymmetric with the progressive addition of Al_2O_3 at the expense of P_2O_5. As the Pauling electronegativity of P (2.19) is higher than that of Al (1.61) [53], it is reasonable to think that the strong P–O bonds have a higher influence on the Er^{3+} site than the Al–O bonds increasing the probability of the 4f-4f transition. It is interesting to notice that the changes in the Er^{3+} absorption and emission band at 1530 nm are more pronounced with the addition of P_2O_5 than with the Al_2O_3 addition confirming the strong role of phosphorus on the Er^{3+} site distortion. The decrease of the relative intensity of the emission band at 1490 nm over the one at 1530 nm

when the Al_2O_3 concentration increases may be explained by a modification of the electronic population of the $^4I_{13/2}$ sub-levels favoring the sub-level at 1530 nm at the expense of the one at 1490 nm. This is also confirmed by the fact that the glasses with x ~ 1 have a higher emission intensity at 1530 nm than the glass with x = 3 while having a similar absorption cross-section at 980 nm but a higher OH content. The local maximum of the absorption cross-section for x ~ 1.5 (Fig. 2d and 2e) is most probably related to the formation of Al–O–P linkages in the network, which are also believed to have a significant Er^{3+} site distorting role. However, while the glass with x = 1.5 exhibits a similar absorption cross-section at 980 nm and a similar OH content that the glass x = 0, the glass x = 1.5 exhibits however a lower emission at 1530nm. This is not fully understood and still under investigation. The low emission at 1530 nm of the glass with x = 3 can be related to the high content in hydroxyl groups as seen in Fig. 3, since it is well know that OH hydroxyl groups are serious quenchers of Er^{3+} ions luminescence [54,55]. Theoretical calculations by the Judd-Ofelt analysis are in progress in order to get a better description of the Er^{3+} coordination environment.

5. Conclusion

The goal of this study was to evaluate the influence of P_2O_5 and Al_2O_3 content on the structure of erbium-doped sodium-borosilicate glasses and also on their physical, thermal, optical and luminescence properties. The addition of P_2O_5 or Al_2O_3 at the expense of B_2O_3 and Na_2O results in an increase of the polymerization degree of the silicate network while the fraction of $^{[4]}B$ increases, with various ratios of neutral and charged $^{[3]}B$ species. These changes in the structure have been related to changes in T_g, n, absorption cross-sections at 1530 nm and 980 nm and also in the emission at 1530 nm. Al and P are strongly suspected to modify the coordination shell of Er^{3+}, thus affecting the optical and luminescence properties. To conclude, the present study has demonstrated the better efficiency of phosphorous rather than aluminium in the declustering process of erbium ions in sodium borosilicate glasses with a low silica content.

Acknowledgments

A part of the research leading to these results has received funding from the European Union Seventh Framework Programme FP7/2007-2013 under grant agreement n°264526 through the GlaCERCo Marie-Curie ITN project. The Finnish Funding Agency for Technology and Innovation (TEKES) is acknowledged by nLIGHT for financial support. The Academy of Finland is gratefully acknowledged for the financial support of J.M.. The help of S. Guastella for the XPS measurements and of A. Venturella for the FTIR measurements is greatly acknowledged.

References

[1] B. E. A. Saleh, M. C. Teich, Fundamentals of Photonics, Wiley, New York (1991).

[2] P. C. Becker, N. A. Olsson, Jay R. Simpson, Erbium-Doped Fiber Amplifiers: Fundamentals and Technology, Academic Press Inc. (London, 1999) Std..

[3] A.J. Kenyon, Progress in Quant. Electr., 26 (2002), 225–284.

[4] S.E. Stokowski, R. A. Saroyan, M. J. Weber, Lawrence Livermore National Laboratory Report M-095 2 (1981).

[5] W.J. Miniscalco, J. Lightwave Technol. 9 (1999) 234–250.

[6] M.M. Bubnov, V.N. Vechkanov, A.N. Gur'yanov, K.V. Zotov, D.S. Lipatov, M.E. Likhachev, M.V. Yashkov, Inorg. Mat. 45 (2009), 444–449.

[7] M. J. Weber, J. Non- Cryst. Solids 123 (1990) 208–222.

[8] S. Jetschke, S. Unger, A. Schwuchow, M. Leich, J. Kirchhof, Opt. Express 16 (2008) 15540.

[9] S. Sen, R. Rakhmatullin, R. Gubaidullin, A. Pöppl, Phys. Rev. B 74 (2006) 100201.

[10] M.J.F. Digonnet, Rare-Earth-Doped Fiber Lasers and Amplifiers, Marcel Dekker, New York (2002).

[11] K. Arai, H. Namikawa, K. Kumata, T. Honda, Y. Ishii, T. Handa., J. Appl. Phys. (1986) 593430–3436.

[12] W.F. Du, K. Kuraoka, T. Akai, T. Yazawa, J. Mat. Sci. 35 (2000) 4865.

[13] E.I. Kamitsos, J.A Kapoutsis, H. Jain, H.S. Hsieh, J. Non-Cryst. Solids, 172 (1994) 31–45.

[14] K. El-Egili, Physica B 325 (2003) 340–348.

[15] M. Okuno, N. Zotov, M. Schmucker, H. Schneider, J. Non-Cryst. Solids 351 (2005) 1032–1038.

[16] D. Moncke, D. Ehrt, C.-P.E. Varsamis, E.I. Kamitsos,A.G. Kalampounias, Proc. Fifth Int. Conf. on Borate Glasses, Crystals and Melts Glass Tech.: Eur. J. Glass Sci. Technol. A 47 (2006) 133–137.

[17] J. Massera, C. Claireaux, T. Lehtonen, J. Tuominen, L. Hupa, M. Hupa, J. Non-Cryst. Solids, 357 (2011) 3623–3630.

[18] A.Quintas, D. Caurant, O. Majérus, T. Charpentier, J.-L. Dussossoy, Mat. Res. Bull. 44 (2009) 1895–1898.

[19] M.E. Likhachev, M.M. Bubnov, K.V. Zotov, O.I. Medvedkov, D.S. Lipatov, M.V. Yashkov, A N Guryanov, Quant. Electr. 40 (2010), 633–638.

[20] D.J. DiGiovanni, J.B.MacChesney, T.Y.Kometani, J. Non-Cryst. Solids 113 (1989) 58.

[21] S.G. Kosinski, D.M. Krol, T.M. Duncan, D.C. Douglass, J.B. MacChesney, J.R. Simpson, J. Non-Cryst. Solids 105 (1988) 45–52.

[22] E.I. Kamitsos, G.D. Chryssikos, J. Molec. Struct. 247 (1991) 1.

[23] W. J. Dell, P. J. Bray and S. Z. Xiao, J. Non-Cryst. Solids 58 (1983) 1.

[24] V.G. Plotnichenko, V.O. Sokolov, V.V. Koltashev, E.M. Dianov, J. Non-Cryst. Solids 306 (2002) 209–226.

[25] H. Li, P. Hrma, J.D. Vienna, M. Qian, Y. Su, D.E. Smith, J. Non-Cryst. Solids 331 (2003) 202–216.

[26] S. Liu, Y. Zhang, W. He, Y. Yue, J. Non-Cryst Solids 357 (2011) 3897.

[27] Y. Yan, A.J. Faber, H. Waal, J. Non-Cryst. Solids 181 (1995) 283.

[28] L. Nemec, J. Gotz, J. Am. Ceram. Soc. 53 (1970) 526.

[29] S.N. Houde-Walter, P.M. Peters, J.F. Stebbins, Q. Zeng, J. Non-Cryst. Solids 286 (2001) 118–131.

[30] S.N.B. Bhaktha, B. Boulard, S. Chaussedent, A. Chiappini, A. Chiasera, E. Duval, C. Duverger, S. Etienne, M. Ferrari, Y. Jestin, M. Mattarelli, M. Montagna, A. Monteil, E. Moser, H. Portales, K.C. Vishunubhatla, Opt. Mat. 28 (2006) 1325–1328.

[31] N. Ollier, T. Charpentier, B. Boizot, G. Wallez, D. Ghaleb, J. Non-Cryst. Solids 341 (2004) 26

[32] A. S. Tenney and J. Wong, J. Chem. Phys. 56 (1972) 5516–5523.

[33] R.J. Bell, A. Carnevale, C.R. Kurkjian, G.E. Peterson, J. Non-Cryst. Solids, 35–36 (1980) 1185–1190.

[34] E.I. Kamitsos, A.P. Patsis, M.A. Karakassides, G.D. Chryssikos, J. Non-Cryst. Solids 126 (1990) 52–67.

[35] E.I. Kamitsos, A.P. Patsis, G.D. Chryssikos, J. Non-Cryst. Solids, 152 (1993) 246–257.

[36] N.M. Vedishcheva, B.A. Shakhmatkin, A.S. Wright, Phys. Chem. Glasses 44 (2003)191–196.

[37] J.E. Shelby, Introduction to Glass Science and Technology, Royal Soc. Chem., 2nd Edition (2005).

[38] D. Chen, H. Miyoshi, H. Masui, T. Akai, T. Yazawa, J. Non-Cryst. Solids 345-346 (2004) 104–107.

[39] V. E. Eremyashev, A. A. Osipov, L. M. Osipova, Glass and Ceramics 68 (2011) 205–208.

[40] G. Gao, L. Hu, H. Fan, G. Wang, K. Li, S. Feng, S. Fan, H. Chen, Opt. Mat. 32 (2009) 159–163.

[41] L. Wondraczek, G. Gao, D. Möncke, T. Selvam, A. Kuhnt, W. Schwieger, D. Palles, E.I. Kamitsos, J.Non-Cryst. Solids 360 (2013) 36–40.

[42] G.D. Chryssikos, E. I. Kamitsos, Proc. Int. Symp. Glass Sci. Tech. (1993) Edited by G. D. Chryssikos & E. I. Kamitsos, Greek Glass Federation, Athens, Greece.

[43] U. Moryc, W.S Ptak, J. Mol. Struct., 511–512 (1999) 241–249.

[44] D. Möncke, M. Dussauze, E. I. Kamitsos, C.P.E. Varsamis, D. Ehrt, Phys. Chem. Glasses: Eur. J. Glass Sci. Technol. B 50 (2009) 229–235.

[45] Y. D. Yiannopoulos, G. D. Chryssikos, E. I. Kamitsos, Phys. Chem. Glasses 42 (2001) 164–172.

[46] Mysen85 B.O. Mysen, D. Virgo, I. Kushiro, Am. Mineral. 70 (1985) 88.

[47] R.K. Brow, D.R. Tallant, S.T. Myers, C.C. Phifer, J.-Non-Cryst. Solids 191 (1995) 45–55.

[48] M. Rokita, M. Handke, W. Mozgawa, J. Mol. Struct. 450 (1998) 213.

[49] M. Rokita, M. Handke, W. Mozgawa, J. Mol. Struct. 555 (2000) 351–356.

[50] 50 L.D. Pye, V.D. Frechette, N.J. Kreidl, Borate glasses: structure, properties, applications ; Plenum Press, New York (1978).

[51] A. Monteil, S. Chaussedent, G. Alombert-Goget, N. Gaumer, J. Obriot, S.J.L. Ribeiro, Y. Messaddeq, A. Chiasera, and M. Ferrari, J. Non-Cryst. Solids 348 (2004) 44.

[52] J. Ding, Y. Chen, W. Chen, L. Hu, G. Boulon, Chin. Opt. Lett. 10 (2012) 071602.

[53] J.E. Huheey, E.A. Keiter, R.L. Keiter, Inorganic Chemistry: Principles of Structure and Reactivity, 4th edition, HarperCollins, New York, USA (1993).

[54] Y. Yan, A.J. Faber, H. de Waal, J.-Non-Cryst. Solids 181 (1995) 283–290.

[55] X. Feng, S. Tanabe, T. Hanada, J. Non-Cryst. Solids 281 (2001) 48.

Table captions

Table 1. Glass composition, label, glass density, absorption coefficient at 3500 cm^{-1}, OH group concentration

Table 2. Values of R (= Na_2O/ B_2O_3), R' (= (Na_2O-Al_2O_3)/B_2O_3), R* (= (Na_2O-P_2O_5-Al_2O_3+2*$AlPO_4$)/B_2O_3), and N_3, N_4, Q^3 and Q^4 fractions calculated by the Dell-Bray-Xiao (DBX) model before and after modification.

Table 1

x	SiO_2 (mol%)	Na_2O (mol%)	B_2O_3 (mol%)	Er_2O_3 (mol%)	P_2O_5 (mol%)	Al_2O_3 (mol%)	$[Er^{3+}]$ ($\times 10^{19}$ ions.cm-3) (±5%)	ρ ($g.cm^{-3}$) (± 0.05)	α (cm^{-1}) (± 5 %)	[OH] ($\times 10^{19}$ $ions.cm^{-3}$) (±5%)
	50	21.82	28.06	0.12			5.81	2.46	3.53	4.34
0	50	20.51	26.36	0.12	3	0	5.31	2.47	5.08	6.25
0.5	50	20.51	26.36	0.12	2.5	0.5	5.31	2.46	7.95	9.77
1	50	20.51	26.36	0.12	2	1	5.27	2.44	8.36	10
1.18	50	20.51	26.36	0.12	1.82	1.18	5.27	2.43	5.36	6.59
1.34	50	20.51	26.36	0.12	1.66	1.34	5.28	2.43	5.46	6.71
1.5	50	20.51	26.36	0.12	1.5	1.5	5.31	2.45	4.91	6.04
1.67	50	20.51	26.36	0.12	1.33	1.67	5.31	2.44	5.09	6.26
2	50	20.51	26.36	0.12	1	2	5.30	2.43	4.93	6.05
2.5	50	20.51	26.36	0.12	0.5	2.5	5.35	2.45	6.50	7.98
3	50	20.51	26.36	0.12	0	3	5.31	2.43	6.37	7.82

Table 2

$x(Al_2O_3)$	R	K	R'	R*	DBX model				Modified DBX model			
					N_3 (%)	N_4 (%)	Q^3 (%)	Q^4 (%)	B_3 (%)	B_4 (%)	Q^3 (%)	Q^4 (%)
Matrix	0.78	1.78	0.78	0.78	0.39	0.61	18.7	81.3	0.39	0.61	18.7	81.3
0	0.78	1.90	0.78	0.66	0.38	0.62	16.8	83.2	0.38	0.62	4.8	95.2
0.5	0.78	1.90	0.76	0.70	0.38	0.62	14.8	85.2	0.38	0.62	8.8	91.2
1	0.78	1.90	0.74	0.74	0.38	0.62	12.8	87.2	0.38	0.62	12.8	87.2
1.18	0.78	1.90	0.73	0.75	0.38	0.62	12.1	87.9	0.38	0.62	14.2	85.8
1.34	0.78	1.90	0.73	0.77	0.38	0.62	11.4	88.6	0.38	0.62	15.5	84.5
1.5	0.78	1.90	0.72	0.78	0.38	0.62	10.8	89.2	0.38	0.62	16.8	83.2
1.67	0.78	1.90	0.71	0.77	0.38	0.62	10.1	89.9	0.38	0.62	15.4	84.6
2	0.78	1.90	0.70	0.74	0.38	0.62	8.8	91.2	0.38	0.62	12.8	87.2
2.5	0.78	1.90	0.68	0.70	0.38	0.62	6.8	93.2	0.38	0.62	8.8	91.2
3	0.78	1.90	0.66	0.66	0.38	0.62	4.8	95.2	0.38	0.62	4.8	95.2

Figure captions

Fig. 1. (a) Refractive index (n_{1312}) at 1312 nm and (b) Glass transition temperature (T_g) versus x (Inset: T_x-T_g difference. For the matrix glass, no crystallization peak was detected). Solid line is a guide for the eye.

Fig. 2. (a) UV-visible-IR absorption spectrum of the Er-doped borosilicate matrix glass. Absorption cross-section spectra at (b) 980 nm and (c) 1530 nm corresponding respectively to the $^4I_{15/2} \rightarrow {}^4I_{11/2}$ and $^4I_{15/2} \rightarrow {}^4I_{13/2}$ transitions (Insets of (b) and (c): normalized spectra), (d) Evolution of the absorption cross-section at 980 nm versus x and (e) Absorption peak integral $A^{Abs}(1530)$ at 1530 nm versus x. Solid line is a guide for the eye.

Fig. 3. IR absorption spectra of some Er-doped borosilicate glasses with various contents of P_2O_5 and Al_2O_3 in the 3000–4000 cm^{-1} range.

Fig. 4. (a) Emission spectra of some Er-doped borosilicate glasses with various contents of P_2O_5 and Al_2O_3 (λ_{exc} = 980 nm) (Inset: normalized spectra) and (b) Emission integral $A^{Em}(1530)$ at 1530 nm versus x. Solid line is a guide for the eye.

Fig. 5. Normalized IR reflexion spectra of the glasses (matrix, x = 0, 1.5 and 3).

Fig.6. (a) Normalized XPS Si2p spectra of Er-doped borosilicate glasses with various contents of P_2O_5 and Al_2O_3 and (b) Si2p binding energy versus x. Solid line is a guide for the eye.

Fig. 7. (a) ^{11}B MAS NMR spectra of the glasses matrix, x = 0, 1.5 and 3, (b) Evolution of the $^{[3]}B$ and $^{[4]}B$ as a function of x. Solid line is a guide for the eye.

Fig. 8. Evolution of the silicate fractions (Q^3 and Q^4) calculated from the Dell-Bray-Xiao model before and after modification

FIG. 1

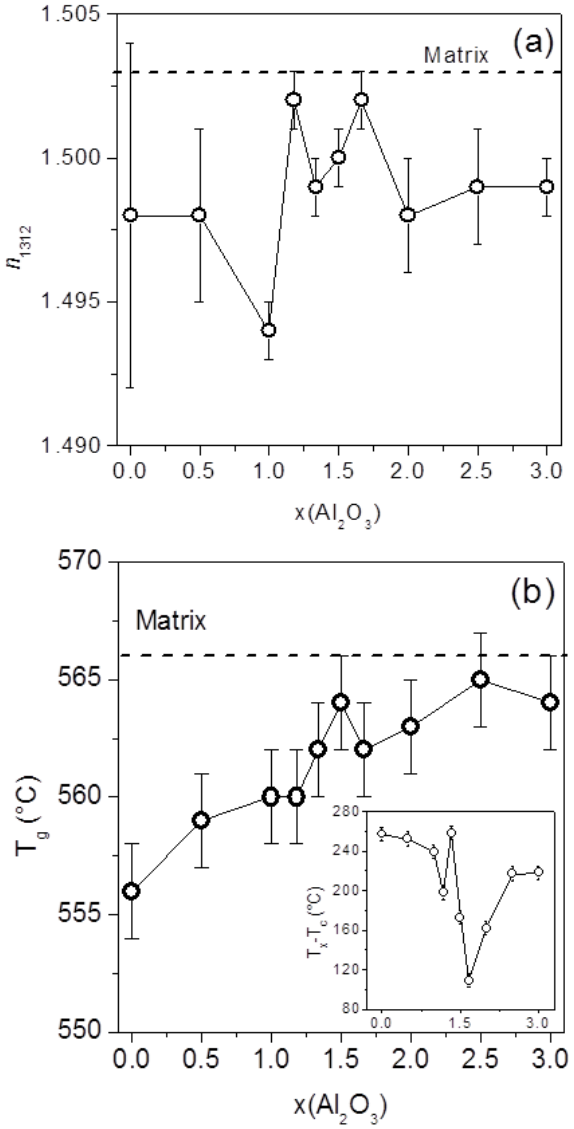
(a)
Matrix
n_{1312}
1.505
1.500
1.495
1.490
0.0
0.5
1.0
1.5
2.0
2.5
3.0
x(Al2O3)
(b)
Matrix
Tg (°C)
570
565
560
555
550
Tx-Tg (°C)
280
240
200
160
120
80

FIG. 2

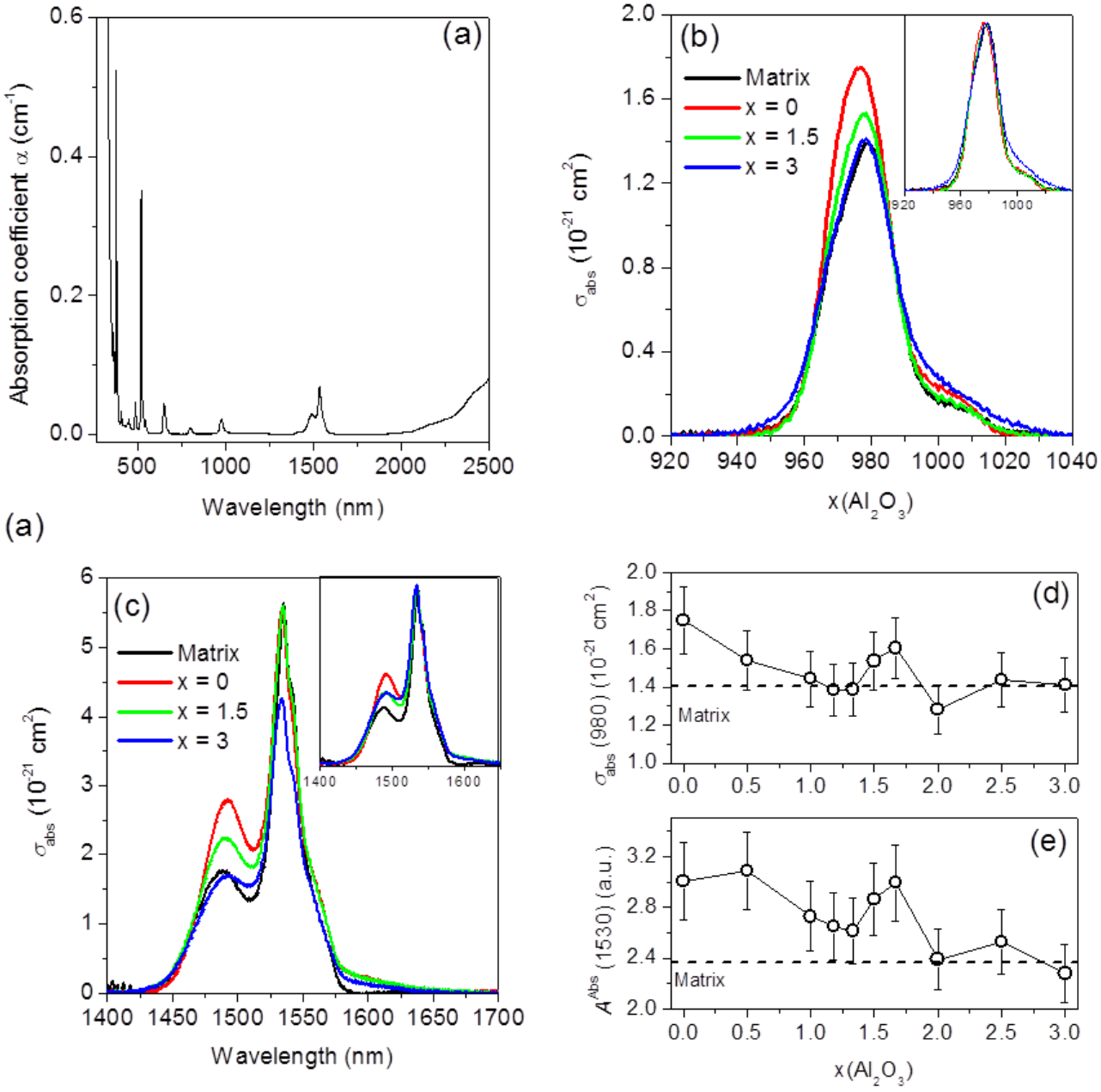
(a)
Absorption coefficient α (cm-1)
Wavelength (nm)
(b)
Matrix
x = 0
x = 1.5
x = 3
σabs (10-21 cm2)
x(Al2O3)
(c)
Matrix
x = 0
x = 1.5
x = 3
σabs (10-21 cm2)
Wavelength (nm)
(d)
σabs (980) (10-21 cm2)
Matrix
(e)
AAbs (1530) (a.u.)
Matrix
x(Al2O3)

FIG. 3

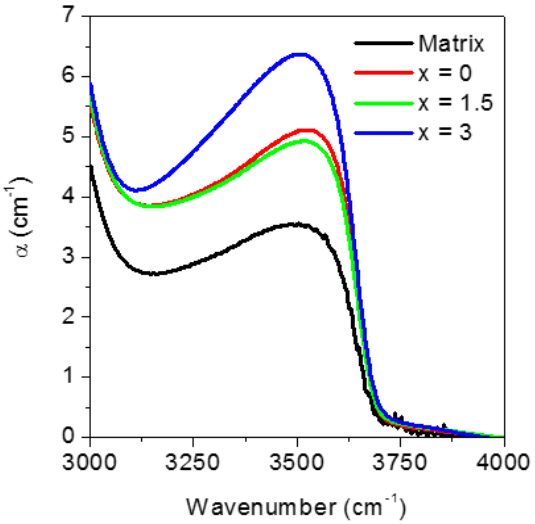
Matrix
x = 0
x = 1.5
x = 3
α (cm-1)
Wavenumber (cm-1)
0
1
2
3
4
5
6
7
3000
3250
3500
3750
4000

FIG. 4

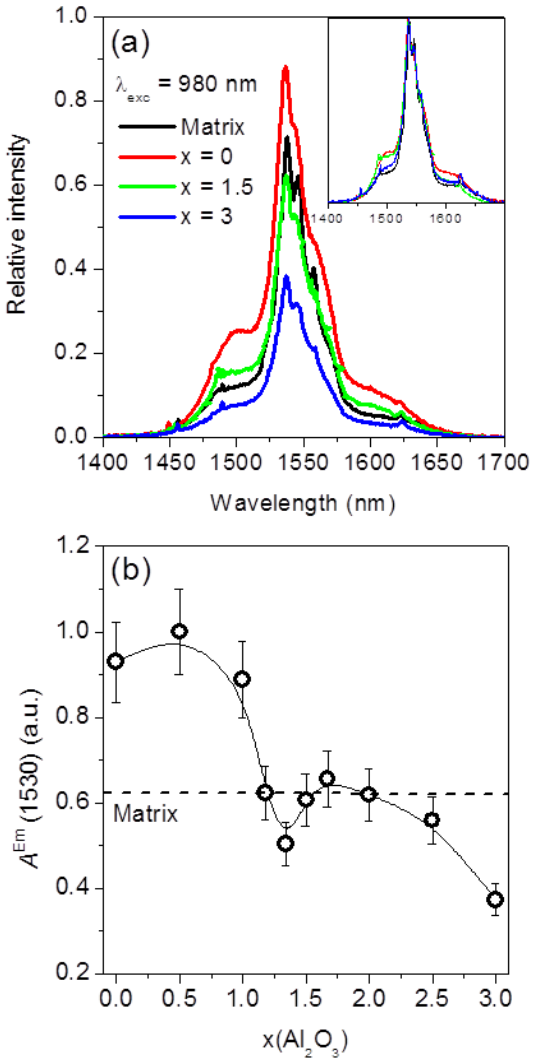
(a)
λexc = 980 nm
Matrix
x = 0
x = 1.5
x = 3
Relative intensity
Wavelength (nm)
(b)
Matrix
AEm (1530) (a.u.)
x(Al2O3)

FIG. 5

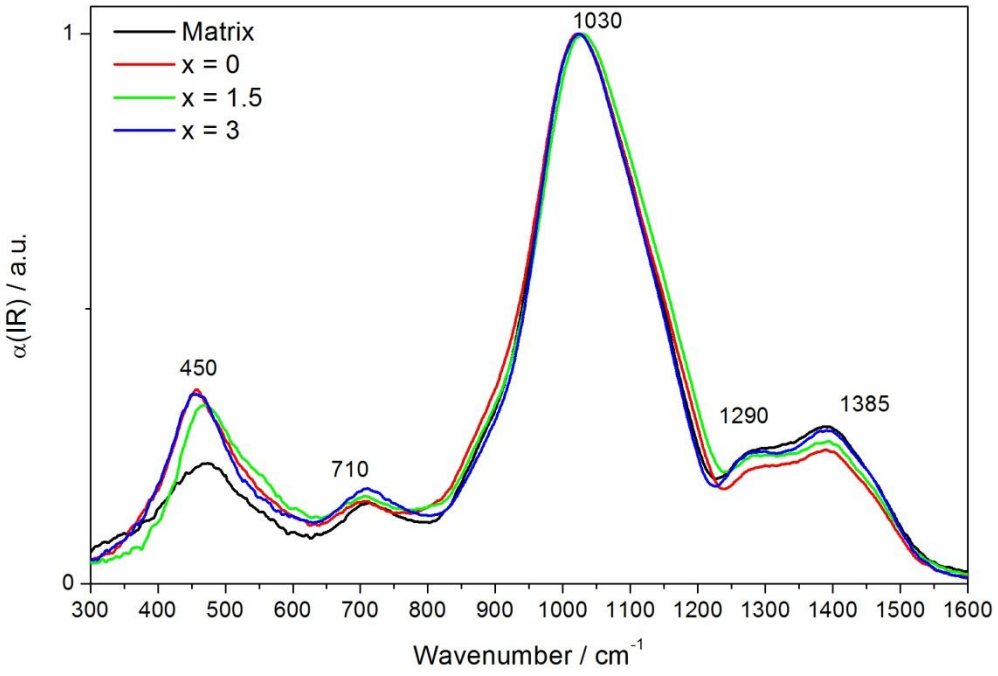
Matrix
x = 0
x = 1.5
x = 3
1030
450
710
1290
1385
1
0
α(IR) / a.u.
300 400 500 600 700 800 900 1000 1100 1200 1300 1400 1500 1600
Wavenumber / cm-1

FIG. 6

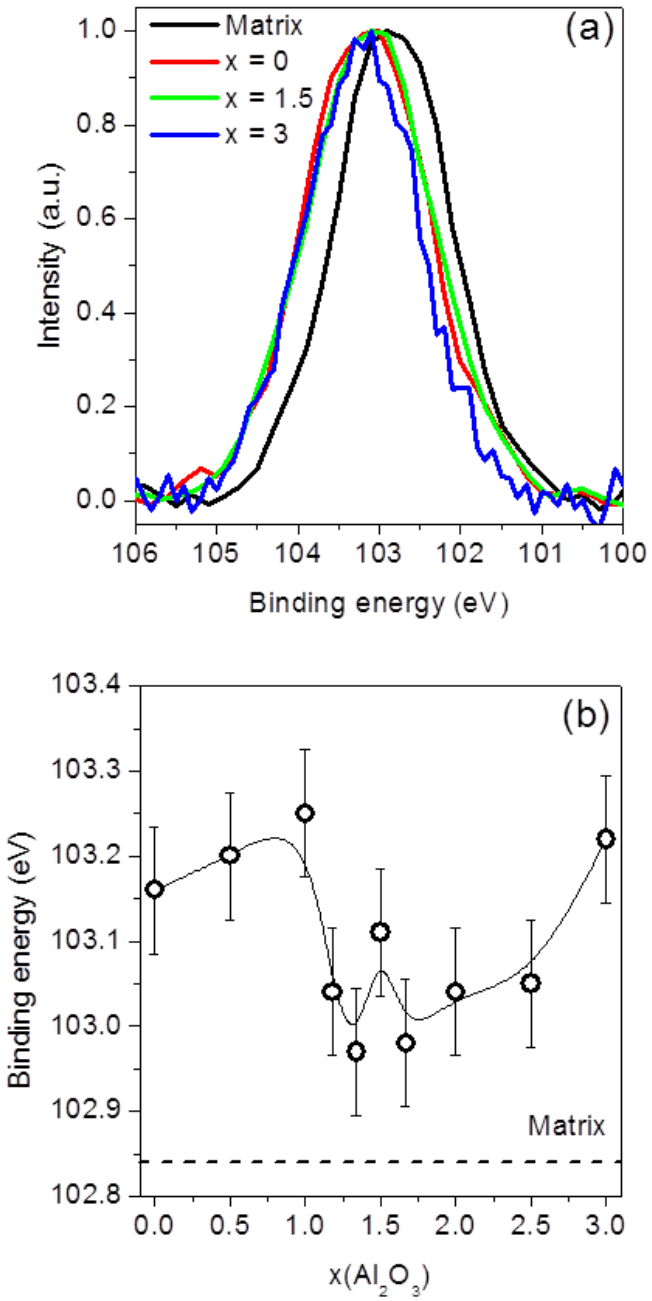
(a)
Matrix
x = 0
x = 1.5
x = 3
Intensity (a.u.)
Binding energy (eV)
(b)
Binding energy (eV)
Matrix
x(Al2O3)

FIG. 7

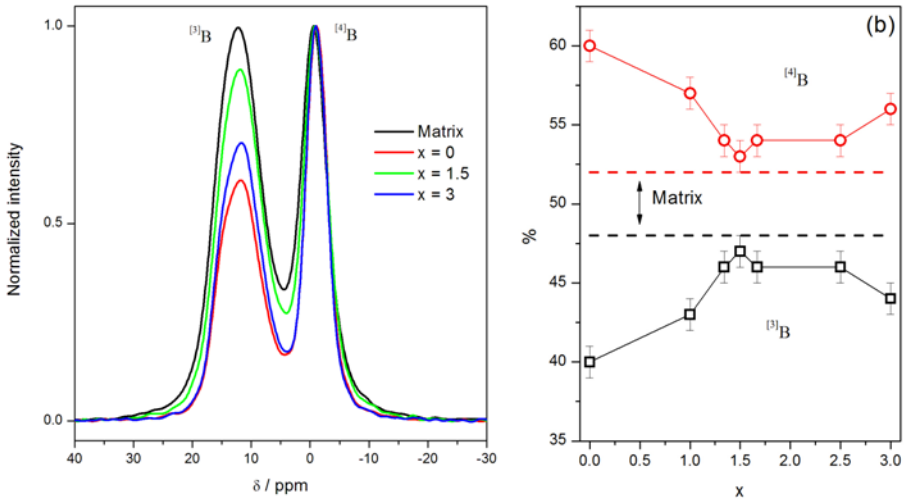

FIG. 8

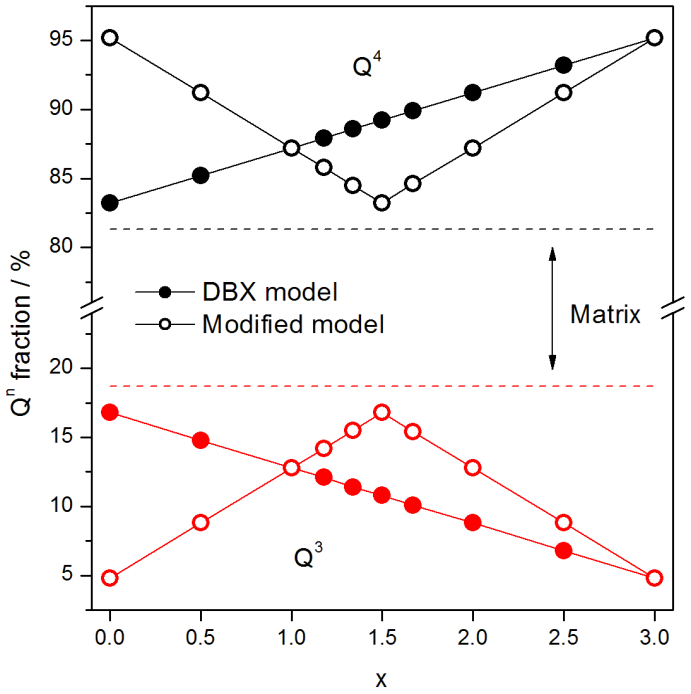
95
90
85
80
20
15
10
5
Q^4
Q^3
DBX model
Modified model
Matrix
Q^n fraction / %
0.0
0.5
1.0
1.5
2.0
2.5
3.0
x